Current-induced skyrmion generation through morphological phase transitions in chiral ferromagnetic heterostructures

Ivan Lemesh,[1] Kai Litzius,[2,3,4] Pedram Bassirian,[2] Nico Kerber,[2] Daniel Heinze,[2] Jakub Zazvorka,[2] Felix Büttner,[1] Lucas Caretta,[1] Max Mann,[1] Markus Weigand,[4] Simone Finizio,[5] Jörg Raabe,[5] Mi-Young Im,[6,7] Mathias Kläui,[2,3,*] and Geoffrey S. D. Beach[1,*]

[1]*Department of Materials Science and Engineering, Massachusetts Institute of Technology, Cambridge, Massachusetts 02139, USA*

[2]*Institute of Physics, Johannes Gutenberg-University Mainz, 55099 Mainz, Germany*

[3]*Graduate School of Excellence Materials Science in Mainz, 55128 Mainz, Germany*

[4]*Max Planck Institute for Intelligent Systems, 70569 Stuttgart, Germany*

[5]*Swiss Light Source, Paul Scherrer Institut, Villigen PSI CH-5232, Switzerland*

[6]*Center for X-ray Optics, Lawrence Berkeley National Laboratory, Berkeley, California 94720, USA*

[7]*Department of Emerging Materials Science, DGIST, Daegu 42988, Korea*

(Dated: August 25, 2017)

Abstract

Magnetic skyrmions promise breakthroughs in future memory and computing devices due to their inherent stability and small size. Their creation and current driven motion have been recently observed at room temperature, but the key mechanisms of their formation are not yet well-understood. Here we show that in heavy metal/ferromagnet heterostructures, pulsed currents can drive morphological phase transitions between labyrinth-like, stripe-like, and skyrmionic states. Using high-resolution x-ray microscopy, we image spin texture evolution with temperature and magnetic field, and demonstrate that transient Joule heating can drive the system across the stripe-skyrmion phase boundary. Our observations are explained through micromagnetic simulations that reveal a crossover to a global skyrmionic ground state above a threshold magnetic field, which we find experimentally to decrease with increasing temperature. We demonstrate how by tuning the phase stability, we can reliably generate skyrmions by short current pulses and stabilize room-temperature skyrmions at zero field, providing new means to manipulate spin textures in engineered chiral ferromagnets.

* Authors to whom correspondence should be addressed: gbeach@mit.edu, klaeui@uni-mainz.de

INTRODUCTION

Magnetic skyrmions represent a class of topological chiral spin textures that can be found in bulk materials [1–3] as well as in ultrathin magnetic films and multilayers [4–6] with perpendicular magnetic anisotropy (PMA). In thin films, skyrmions can exhibit sub-nanometer scale size [7] and move in response to an applied current with velocities exceeding 100 m/s [4] in a controllable [8, 9] and reliable [9] way. For this reason, they promise great technological utility for logic gates [10] and racetrack-type memory devices [11], for which they have to be readily created and manipulated. Homochiral skyrmions can be stabilized by the Dzyaloshinkii-Moriya interaction (DMI) [12, 13] in materials with strong spin orbit coupling and broken inversion symmetry, such as the bulk B20 compounds [1] where they were first discovered. More recently it has been found that a strong interfacial DMI can stabilize skyrmions in asymmetric multilayer stacks of a ferromagnet and a heavy metal [4–6]. Since such systems can also exhibit large current-induced spin-orbit torques that provide an efficient means to create and manipulate [14–16] them, skyrmions in thin metallic multilayers and, in particular, their controlled generation and manipulation are now a central focus of current research.

Magnetic skyrmions can exist as metastable, isolated topological excitations [17, 18], or as ordered arrays (lattice) comprising the magnetic ground state, depending on material and environmental parameters. In the latter case, their mutual interactions tend to lead to formation of a triangular lattice [2, 19], though even in the absence of pinning such order can be easily destroyed [20]. The skyrmion lattice phase resides in a well-defined pocket of temperature-field space, separated from other morphological phases such as the spin-spiral and uniform ferromagnetic states. Transitions amongst these phases have been well-characterized in bulk helimagnets, but less so in applications-relevant ferromagnet/heavy-metal heterostructures [4], where the recent focus has mainly been on room-temperature behavior of isolated skyrmions. In such materials, skyrmion creation has been demonstrated using inhomogeneous in-plane currents in planar structures with patterned constrictions [21, 22], or at defects due to the action of current-induced spin-transfer or spin-orbit torques [16, 23–25]. However, these mechanisms rely on extrinsic effects and the existing studies provide little insight into the energetics and stability of skyrmions with respect to other topological and morphological phases. Moreover, although the large current densities involved often

result in significant Joule heating, most studies have either completely ignored the role of temperature or considered it trivially, only as the source of the variation of magnetic parameters, in understanding the mechanism of skyrmion formation.

Recent work [15] has demonstrated that current-induced Joule heating can play a critical role in nucleating magnetic skyrmions in the multi-domain state in heavy-metal/ferromagnet multilayers, but the mechanism remained unclear. However, it is exactly the underlying physical processes that need to be understood in order to engineer the controlled generation and manipulation of topologically non-trivial spin structures. Here, we provide a mechanistic understanding of the generation of various morphological phases, of their relative stability, and of the thermally-driven transformations between them. Our findings have practical applications, including the creation and current-driven motion of zero-field skyrmions, and reliable skyrmion generation using single current pulses with a duration down to a few ns. We use high-resolution scanning transmission x-ray microscopy (STXM) to image the domain states in ultralow-pinning Pt/CoFeB/MgO multilayers as a function of temperature and magnetic field. We identify several distinct morphological phases, including labyrinth-like, stripe-like, and skyrmionic phases, and show that injected current pulses can be used to drive transitions amongst these states in a controllable way. We find that in these ultralow-pinning materials, it is mainly the peak transient sample temperature that defines the morphology of the final state, with current-induced torques — in contrast to previous claims and common expectations — playing a minor role. We demonstrate directly how the skyrmion generation occurs through an intrinsic phase transformation mediated by development of morphological instabilities. This work yields key insights into phase stability in chiral ferromagnets and provides a practical means to generate magnetic skyrmions on demand without using extrinsic defects [24, 25], which would act at the same time as unwanted pinning centers thereby complicating the device operation.

RESULTS

Imaging magnetic textures with X-ray microscopy

We examined $[Pt(2.7\ nm)/CoFeB(0.86\ nm)/MgO(1.5\ nm)]_{\times 15}$ multilayers grown by sputter deposition and patterned into 2-micron wide tracks with contacts at either end

for electrical current pulse injection (see Methods). The resulting material (Fig. 1a) exhibits strong PMA with a hysteresis loop shown in Fig. 1b, where the low zero-field remanence implies a multidomain state. Due to the structural inversion asymmetry, such stacks are known [4, 9] to exhibit a large net DMI. We find a DMI constant $D \approx 1.2$ mJ/m^2 for the present films (see Methods), which is sufficient to ensure a homochiral Néel texture for domain walls and skyrmions (see Supplemental Information), as evidenced experimentally below. It has previously been shown that this material exhibits highly reproducible current-induced skyrmion motion [9, 26] due to its homogeneity and low pinning profile. Here, we employ temperature-dependent static magnetic imaging of the domain states using STXM, as shown schematically in Fig. 1c, to examine current-driven transitions and stability of the magnetic textures in this ultralow-pinning system.

First, we reveal the distinct room temperature magnetic states that the system exhibits, which can be accessed through current-pulse excitation under various magnetic bias fields. Prior to all measurements we apply an alternating-field demagnetization cycle, which yields an initial multidomain state with a labyrinth character as depicted in Fig. 1d. The effects of the application of a train of 10000 bipolar current pulses with the voltage of 2.6 V and pulse width of 7.5 ns (corresponding to a current density $J \approx 4.3 \times 10^{11}$ A/m^2), are shown in Figs. 1e-g for increasing values of the out-of-plane (OOP) field. Here, bipolar pulses are used instead of unipolar pulses to minimize current induced displacement and highlight current-induced changes to the magnetic state. At zero field, the labyrinth structure evolves into a system of parallel stripes, as can be seen in Fig. 1e. The stripes can align either parallel or orthogonal to current flow depending on the applied voltage (see Supplemental Information for further discussion). As long as the applied field is held at zero, no further evolution occurs upon subsequent current-pulse injection of the given amplitude once the system reaches the orthogonal stripe state. However, if the same pulse excitation is applied in conjunction with a finite out-of-plane magnetic field, skyrmions are produced (Figs. 1f,g), either coexisting with stripes at lower field (Fig. 1f) or as a disordered array at higher field (Fig. 1g). We find that skyrmions are generated regardless of the initial state as long as the current density is above some threshold value $j_{\mathrm{thr}}^{\mathrm{sky}}$ (which is dependent on magnetic field and temperature) and the field is below the saturation value.

Figures 1h,i show that the effects of current pulses are cumulative, and that with fewer pulses injected (here 100 pulses, with similar characteristics as in Figs. 1e-g), the transition

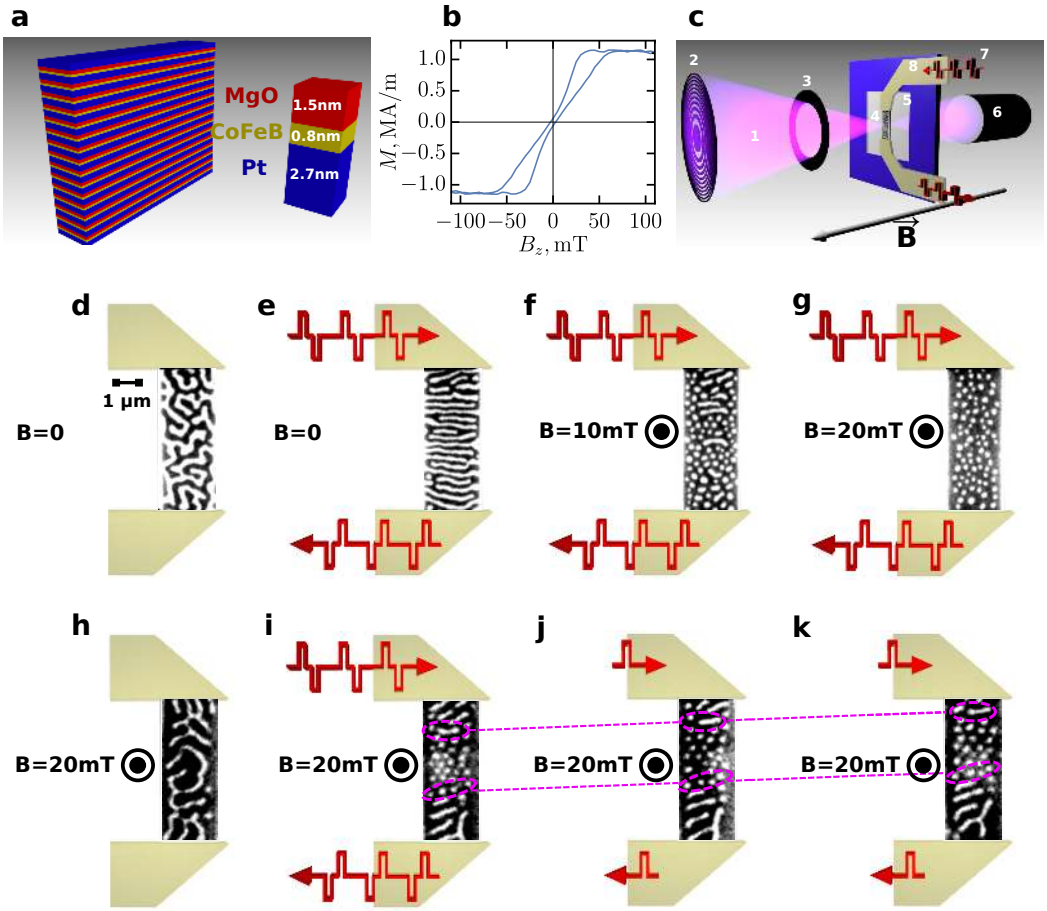

Figure 1 | Experimental setup and the effect of the applied field and current pulse excitation. **(a)** Schematic multilayer stack of Pt/CoFeB/MgO with 15 repeats and **(b)** measured out-of-plane hysteresis loop. **(c)** Experimental schematic of the setup used for scanning transmission X-ray microscopy (STXM) experiments: An x-ray beam (1) is focused with a zone plate (2) on the sample (4) located on (5) a SiN membrane in the presence of an applied out-of-plane magnetic field. An order selecting aperture (3) is employed to pass the first order diffraction and to avoid the illumination of the sample from the zero-order light. The transmitted beam is collected at the detector (6). The current pulses (7) are injected through gold pads (8) that are connected to the sample. **(d-g)** Magnetic states resulting from the application of trains of 10000 bipolar pulses with 7.5 ns pulse width and (transmitted) pulse amplitude $V = 2.6\ V$ to the initial demagnetized state **(d)** leading to **(e)** the aligned stripe state, **(f)** the mixed state, and **(g)** the skyrmion state. Another mixed state **(i)** has been achieved by applying a train of 100 pulses with $V = 2.7\ V$ and 5 ns pulse width from the initial labyrinth state **(h)** at 20mT. **(j-k)** The subsequent homogeneous motion has been induced by the repeated application of single unipolar pulses with $V = 3.6\ V$ and 5 ns pulse width.

to the skyrmionic state is incomplete. The state in Fig. 1i allows us to conveniently probe the effects of current-induced spin-orbit torques on domain walls and skyrmions simultaneously, and to identify their homochiral nature and low-pinning behavior. As seen in 1j,k, single unipolar current pulses act to uniformly displace both the stripe domains and the skyrmions, in a direction opposite to electron flow, consistent with the expected behavior for left-handed chiral Néel domain walls and skyrmions under the action of the damping-like torque induced by spin accumulation due to the spin Hall effect in Pt [27, 28]. The concurrent and synchronous displacement of all magnetic features indicates an absence of strong pinning centers within the patterned structure, as also evidenced in prior pump-probe experiments on this material [9].

Threshold current for skyrmion creation

For applications, the generation of skyrmions is the key step and therefore we focus next on understanding the conditions leading to pulsed-current skyrmion generation. For this, we fix the value of the applied out-of-plane magnetic field to 40 mT (at which a skyrmion lattice can be easily accessed), and vary the current pulse characteristics. Figure 2a depicts the result of applying bipolar pulse trains as a function of pulse amplitude. One can observe a sharp transition to the skyrmion state at the pulse voltage of $V_{\mathrm{thr}}^{\mathrm{sky}} \approx 1.8\ V$ (corresponding to $j_{\mathrm{thr}}^{\mathrm{sky}} \approx 3.0 \times 10^{11}\ \mathrm{A/m^2}$), with no variation of the morphology for larger voltages. If the applied voltage is such that $j < j_{\mathrm{thr}}^{\mathrm{sky}}$, the domains readjust their position, but the intrinsic morphology of the labyrinth/stripe state remains the same. We observe that the total area of the skyrmions is generally equal to the total area of stripe-like domains prior to the transition, suggesting that the latter evolve from the former instead of through nucleation from the uniform state. This in turn suggests that the current plays a direct role in transforming the domain morphology.

Since current can apply both a torque (due to spin-orbit effective fields) and energy (due to Joule heating), we have varied the pulse shape characteristics to determine the dominant driver of the morphological transition. Figure 2b shows the results of a series of experiments in which we decrease the voltage amplitude of the bipolar pulse trains, but increase the pulse width to maintain an identical Joule dissipation. The amplitude of the shortest-duration pulses is chosen to be safely above the threshold identified in Fig. 2a. We find that all the

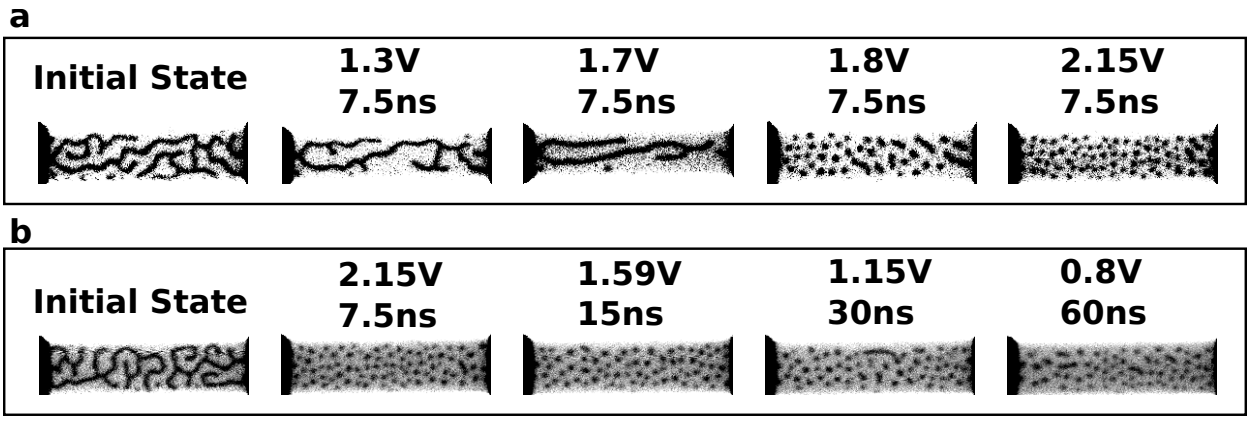

Figure 2 | Skyrmion lattice transition for pulses of different amplitude and width. The evolution of the initial labyrinth structure at 40 mT out-of-plane field: **(a)** as a function of the transmitted voltage of the bipolar pulses with a fixed pulse width of 7.5 ns and **(b)** as a function of the voltage and pulse width, chosen to maintain constant Joule dissipation. In both cases, bipolar pulse sequences consist of 10000 repeats with 1 μs separating each individual unipolar pulse. Each subsequent measurement is taken after a short demagnetizing procedure in order to reset the state (denoted as the initial state).

final states are equivalent, regardless of current pulse amplitude, even when the amplitude is less than half of the threshold suggested by Fig. 2a. Since the experiments in Fig. 2b are all isothermal by design, this result indicates that the threshold current for skyrmion generation is not intrinsic and is hence not related to a threshold torque, thereby identifying a mechanism that is distinct from torque-induced nucleation that was previously identified in zero K simulations [24, 25]. Indeed, since a transformation induced by torques should occur on dynamical timescales of order 1 ns, a comparison of the third panel in Fig. 2a and the fifth panel in Fig. 2b is revealing: as the current-induced torque at V=1.7 V (Fig. 2a, panel 3) is already insufficient to generate skyrmions alone, and the torque at 0.8 V (Fig. 2b, panel 5) is less than half as strong, then its role in generating skyrmions in these experiments must be negligible. Instead, these results suggest that the transition to a skyrmionic state is thermally induced, suggested previously in Ref. 15 based on similar experiments.

Role of temperature in skyrmion creation

Having established the importance of thermal energy in driving the transition from stripe-like domains to skyrmions, we take the next step, which is to directly examine the role of sample temperature in the process by performing experiments at varying substrate temperatures, using a temperature-controlled cryostat. We begin by applying an increasing number of bipolar pulse trains of fixed amplitude and at constant magnetic field as presented in Fig. 3a. We observe that for these pulse parameters, single pulses are insufficient to generate skyrmions, but as the number of pulses increases, skyrmion generation is eventually observed. A key observation is that the number of pulses required depends strongly on the nominal substrate temperature. At 334 K it only takes a few pulses to trigger the skyrmion transition, while at 243 K, even the application of 10000 pulses generates only a few skyrmions. These results suggest that there is a critical temperature at which the skyrmion transition occurs, and that the energy of a single pulse does not heat the sample enough at these substrate temperatures, but cumulative heating by multiple pulses sufficiently raises the sample temperature. This can enable the transition if the combination of the substrate temperature and Joule heating induced temperature rise is sufficient (see Supplemental Information for an estimate of the Joule heating during pulse excitation). This also allows us to understand the observation in Fig. 1i wherein the partial generation of skyrmions occurs away from the contact pads, which are expected to act as heat sinks so that the temperature near the middle of the wire is higher than at its ends where stripes remain.

One can anticipate then that single, short current pulses should generate skyrmions if the amplitude is large enough to heat the sample beyond the skyrmion transition temperature. This is demonstrated in Fig. 3b, in which we apply a single unipolar pulse of fixed 2.9 V amplitude with increasing pulse width, and find that a 6 ns-long pulse completely transforms the system to a skyrmionic state.

Role of magnetic field in establishing the equilibrium phase

To understand the origin of the observed morphological transitions, we now examine the energetics of the labyrinth, stripe, and skyrmion phases versus the magnetic field, which we find in Fig. 1 to be critical in determining the final state after current-pulse excitation. The

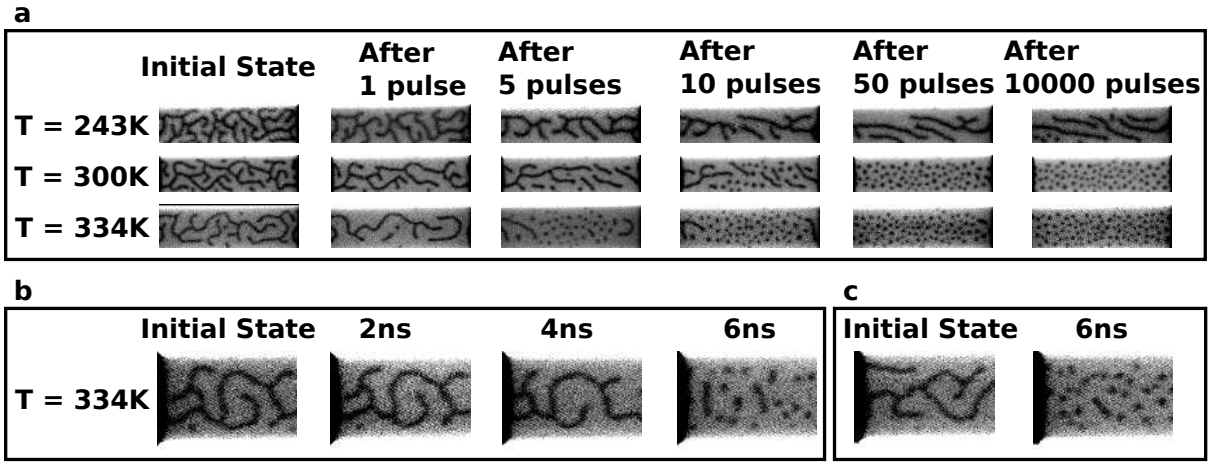

Figure 3 | Skyrmion generation as a function of substrate temperature and the number of applied pulses. The evolution of the initial labyrinth state at 40 mT: **(a)** As a function of temperature for sequences of images acquired after increasing numbers of bipolar pulses of $V = 2.15\ V$ and the individual pulse duration of 7.5 ns. **(b-c)** As a function of the width of a unipolar single pulse of 2.9 V amplitude. Sequence **(c)** depicts a direct single pulse transition to the skyrmion lattice state.

total energy of the system

$$E_{\text{tot}} = E_{\text{anis}} + E_{\text{exch}} + E_{\text{dmi}} + E_{\text{Zeeman}} + E_{\text{mag}} \tag{1}$$

consists of the magnetocrystalline anisotropy energy E_{anis}, exchange and DMI energies E_{exch}, E_{dmi}, respectively, Zeeman energy E_{Zeeman}, and magnetostatic energies E_{mag}. Although simple analytical approximations can be derived for most of the local energy terms [29], no expression exists for the (non-local) magnetostatic energy of the skyrmion lattice state, as it contains analytically-intractable inter- and intra-skyrmion volume and surface stray field interactions that cannot be accurately reduced to simple integrals for the film thicknesses studied here. Such expressions exist only for isolated skyrmions [16], which, however, we cannot apply here due to a close distance between skyrmions in the lattice. Therefore, we employ micromagnetic simulations to compare the total energies of the trigonal skyrmion lattice state, parallel stripe state and labyrinth state (Figs. 4a-c), as a function of out-of-plane field. The results of such simulations using the experimental material parameters (see Methods), are depicted in Fig. 4d, e. For each phase the energy at a fixed field was minimized with respect to the lengthscale of the spin texture (e.g., lattice spacing for the

skyrmionic state). The energetics showing this minimization is depicted in Fig. 4d. This minimum, for each of the three phases, is plotted versus field in Fig. 4e. One sees that the ground state of the system transitions from the ordered stripe phase to the skyrmions lattice phase as the out-of-plane field crosses a threshold B_{thr} (30 mT in Fig. 4e), and that the labyrinth state is always the highest in energy, no matter what field is applied.

Although the ground state is always well-defined, the other states represent local energy minima that can be metastable. As described in Ref. 19, the transitioning between states with different morphologies requires overcoming energy barriers due to the creation of intermediate high-energy states. We have already seen that the initial state in our experiments is always a higher energy labyrinth state. Such a state develops even in the absence of pinning [1] due to a combination of the field inhomogeneities, geometry and original magnetization pattern (if the sample was not fully saturated), which during the demagnetization cycle act together to form a labyrinth pattern [19, 20]. By heating the system (via either current-induced Joule heating or sample heating), we enable the system to overcome such barriers and access transitions between the different states.

To explore the variety of available phases in our fabricated low-pinning Pt/CoFeB/MgO multilayer wires, we introduce pulse trains of different amplitude and vary the applied magnetic OOP-field and the substrate temperature. The pulse sequence consists of 10000 bipolar pulse excitations with a period of 2 μs and the distance between bipolar pulses of 1 μs. Each individual pulse has a width of 7.5 ns with a sub-nanosecond rise time. Figure 4f depicts the morphology that results from applying such pulse trains as a function of applied OOP field (B), substrate temperature (T), and transmitted voltage (U). In the provided diagram, the magnetic states for a specific field and temperature are obtained in a successive manner: starting from an initial state (at 0 V), pulses are injected with increasing amplitude (without re-initializing) and images are acquired at every step. We follow this procedure as an alternative to demagnetizing and resetting the state each time to allow for a complete set of measurements within the limited beamtime at the synchrotron. Nevertheless, as we have identified from numerous measurements, the characteristic morphology of the states derived from such a successive procedure is identical to the one obtained directly from the initial demagnetized state.

[1] In real samples, grains and weak local changes of material parameters also contribute to the formation of labyrinth patterns

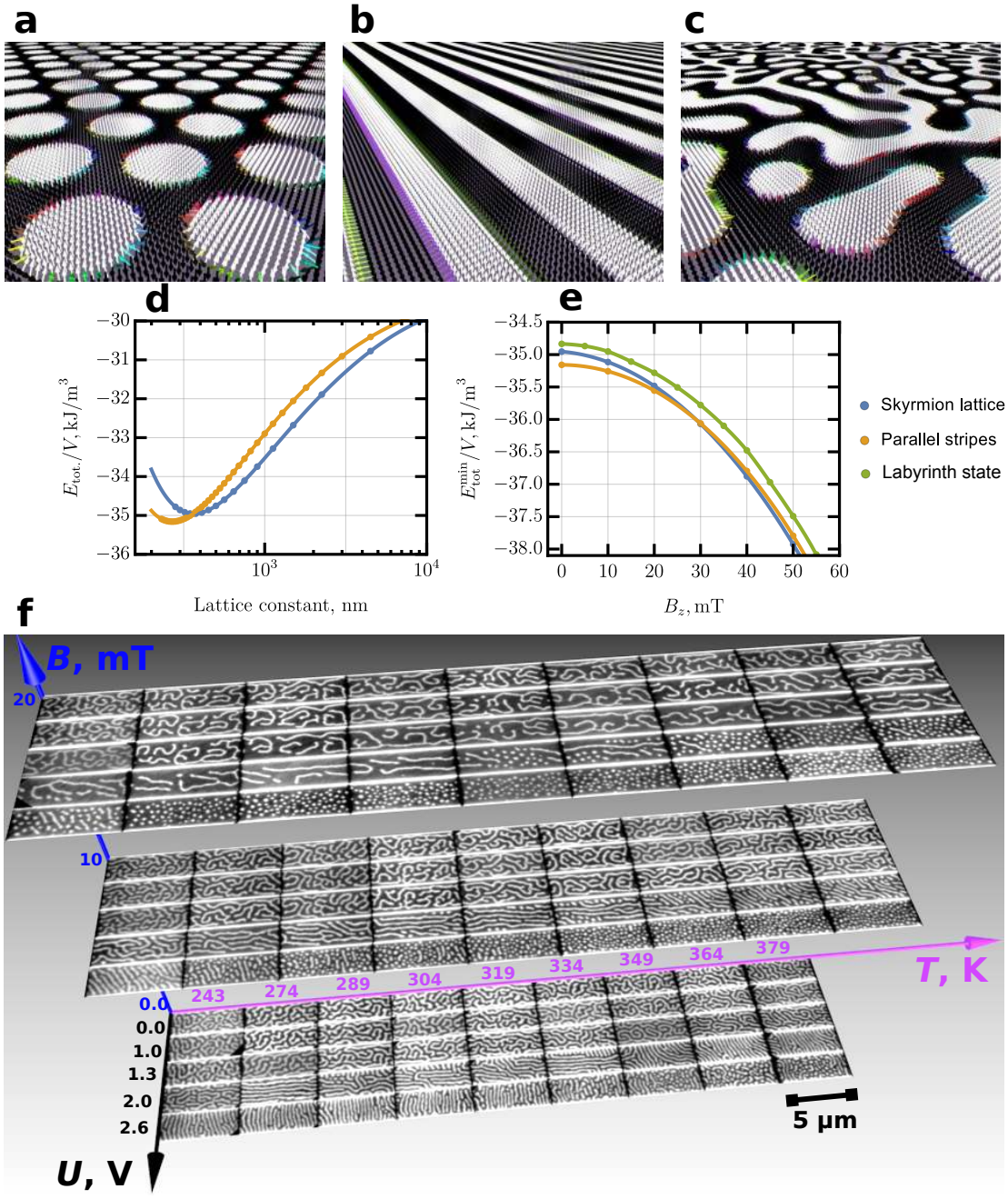

Figure 4 | Simulations of the energetics of various morphological magnetic states. **(a-c)** Simulated spin textures equilibrated with respect to the domain spacing, the domain size and the domain wall width: **(a)** trigonal Néel skyrmion lattice, **(b)** periodic parallel stripe domains and **(c)** labyrinth domains. **(d)** Energy of stripe and skyrmions lattice phase at zero field and various domain density, which is used to determine the equilibrated states (by the lattice constant in the case of stripes we refer to the stripes periodicity λ). **(e)**. The total energy of the equilibrated states versus out-of-plane bias field. **(f)** Experimental B-T-U phase diagram for low-pinning mutliayer stacks of Pt/CoFeB/MgO.

As we can observe from the diagram, the labyrinth state remains unchanged for voltages below 1.3 V, which, in line with our earlier discussion, is likely due to an insufficient thermal energy to overcome the morphological and pinning barriers (the pinning, though small, is still finite in our system). Remarkably, the threshold field $B_{\mathrm{thr}}^{\mathrm{sky}}$ for obtaining skyrmions decreases at high temperatures. The B-T slice at the the maximum voltage of 2.6 V represents a particular interest, as for temperatures above 350 K skyrmions can be found even at zero field.

Zero-field skyrmions

Finally, we demonstrate that based on knowledge of the field- and temperature-dependent phase stability, one can controllably transition between stable and metastable states using fields and applied currents to generate desired states dynamically. We use as an example the generation and current-induced motion of skyrmions at room temperature and zero applied field, which, as shown before, are not the ground state under these conditions. We first generate a skyrmionic state from the demagnetized labyrinth state at an out-of-plane field of 20 mT, which shifts the ground state configuration from stripes to a skyrmion lattice (Figs. 5a,b). The temperature rise enables the system to reach the new ground state, and after subsequently removing the field, the skyrmions indeed survive (Fig. 5c). Their radius, though, increases in order to decrease the net magnetostatic energy. These zero-field skyrmions can subsequently be displaced by unipolar current pulses (Fig. 5c-d) as long as the Joule heating is low enough to prevent recovery of the stripe-like ground state. This transition is evident after the application of bipolar pulse trains (Fig. 5e), where the cumulative heating eventually changes the morphology of the system into the parallel stripes state.

By comparing the states in Fig. 5b and Fig. 5h, we can observe that the skyrmion lattice can be generated from any initial magnetic state. Note that the skyrmionic state remains stable as long as a sufficient magnetic field is applied, no matter how many or how large in amplitude the current pulses are. This implies that the reliability of current-driven skyrmions motion can be enhanced using external bias fields, which increases their stability with respect to other possible states.

Finally, as shown in Fig. 5j (and at the high temperature region of Fig. 4f), even sta-

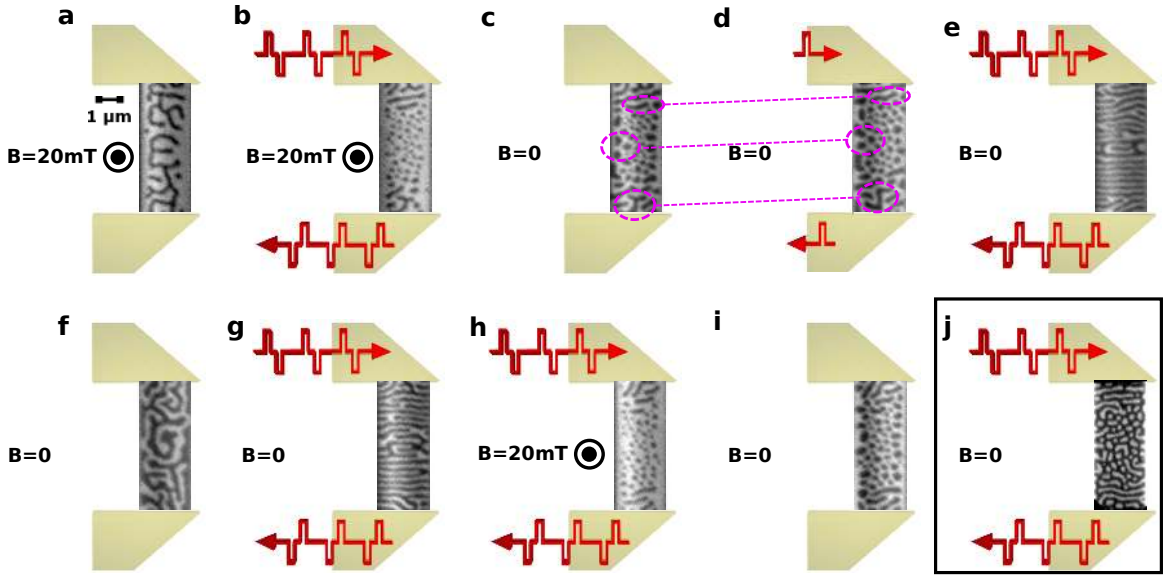

Figure 5 | Generation and current-induced motion of zero-field skyrmions. **(a-e)** The generation of metastable zero field room-temperature skyrmions from **(b)** a magnetized (stable) skyrmions state, which, in turn, has been directly obtained by applying 100 bipolar pulses of 2.7 V to a **(a)** labyrinth state. **(c)** Zero field metastable skyrmions achieved by removing the out-of-plane field. **(c, d)** The uniform motion of zero-field skyrmions after the application of three unipolar pulses of 2.7 V amplitude and 5 ns duration. **(e)** The subsequent stable stripe state that was created from the application of bipolar pulses to such metastable skyrmions state. **(f-i)** The generation of metastable zero field room-temperature skyrmions **(i)** from the stable skyrmion state **(h)**, which in turn was obtained from **(g)** a zero field stripe state. **(j)** Stable zero field skyrmions (mixed with stripes) that were attained at the substrate temperature of 379 K (see Fig. 4f for more details) by application of pulse trains directly to the 0 mT initial state.

ble zero field skyrmions can be achieved in our material. This, however, requires heating the substrate externally to at least 350K prior to applying the bipolar pulse trains. Unlike the metastable zero-field skyrmions mentioned earlier, such high-temperature zero-field skyrmions can survive the application of any pulses, though we find that, as expected, damage to the wires becomes more likely at higher temperatures. The existence of such stable zero-field skyrmions indicates that at higher temperatures, the point of the skyrmionic transition B_{thr} indeed shifts to lower magnetic fields.

DISCUSSION

Our results show that skyrmions in multilayers can occur as a distinct morphological magnetic phase, with a clear phase transition depending on the sample temperature and the magnetic field. We observe that the stripe-to-skyrmion transition can be initiated using transient Joule heating by charge current injection, and that it becomes favourable for applied currents above the (temperature-dependent) threshold $j_{\mathrm{thr}}^{\mathrm{sky}}$ and for fields above B_{thr}. In the Supplemental Information we also demonstrate similar properties for aligned stripes, in which we find that a labyrinth-to-stripes transition occurs only above the threshold current $j_{\mathrm{thr}}^{\mathrm{str}}$. The stripe state, as we show there, can also be obtained from a labyrinth state after just a single nanosecond-long pulse. We generally find that homogenous currents delivering the same amount of Joule heating always lead to equivalent morphologies of the final state, as long as the applied field and the substrate temperature are fixed. As can be seen in Fig. 4f, some of these morphologies exist only in a small pocket of applied voltages and fields. We therefore conclude that it is mainly the sample heating by the injected current that controls the morphology of the generated state.

Generally, such skyrmionic, labyrinth, and stripe domain morphologies exist not only in multilayers, but also in many other systems [30] with short-range attractive and long-range repulsive interactions. The transitioning between such modulated phases is usually impeded by high-energy intermediate states [19]. However, morphological instabilities in such systems can lead to the shape distortions of magnetic textures that eventually can result in the transitioning between such states [20]. For instance, in thin magnetic films with confined geometries, it has been found that a morphological stripe-to-bubble transition can be driven by the inhomogeneous distribution of currents exerting spin-orbit torques [21]. In magnetic garnet films, stripe-to-bubble transition has been observed near T_c [30], and suppressed at lower temperatures. Stripe-to-skyrmion transition have also been observed as a function of applied field and temperature in bulk chiral helimagnets [3] and in symmetric Fe/Gd ferrimagnetic multilayers [31]; our work however constitutes the first experimental demonstration that a similar phase space exists in high-DMI metallic thin film systems at high temperatures.

We, hence, can link our thin film multilayers to these earlier studies and treat stripe and

skyrmionic morphologies as distinct phases. We argue that the phase transformation [2] in our system occurs at a net peak temperature of the system defined as:

$$T^{\max}_{\text{substrate}} = T^{\text{avg}}_{\text{substrate}} + \Delta T^{\max}_{\text{Joule}}, \tag{2}$$

where $T^{\text{avg}}_{\text{substrate}}$ is the average sample temperature given by the heating due to the cryostat heater and the residual heat from previous pulses, $\Delta T^{\max}_{\text{Joule}}$ is the maximum temperature increase, occuring during the pulse transmission. From our resistance measurements during the experiment, we find that the increase of the average temperature $T^{\text{avg}}_{\text{substrate}}$ during the excitation by bipolar pulse trains never exceeded 10 K, which is no surprise as we always kept a low duty cycle of $0.5-0.7\%$ leading to the average injected power of 1 mW. However as we find from our real-time heating measurements (see Supplemental Information), fabricated wires heat up by $\Delta T^{\max}_{\text{Joule}} \approx 70\ K$ during the transmission of a pulse[3]. As was pointed out in earlier works [30, 33, 34], an increase in the substrate temperature (remaining below the Curie temperature T_c) can significantly facilitate the transition from the stripe to the bubble-like morphology. Therefore, the resulting phases that we observe after applying pulses are likely metastable with respect to the sample temperature $T^{\text{avg}}_{\text{substrate}}$, but stable with respect to $T^{\max}_{\text{substrate}}$. Nevertheless, as we have already found for metastable zero-field room-temperature skyrmions, not only do such phases exist in multilayers, but they also can be uniformly displaced in response to the current injections.

In our multilayers, we observe that the transition from stripe domains to skyrmions as a function of field and temperature qualitatively follows the established trend in field-temperature phase diagrams of the stripe-to-bubbles transitions [35] and of helical-to-skyrmionic transitions [3] in bulk B20-compounds. However, for future studies it would be desirable to explore the phase diagram of multilayers at a greater depth, (especially at temperatures approaching T_c) with finer steps in applied field, temperature and currents, and importantly, by tracking the real-time temperature of the sample during the pulse injection. This is, however, beyond the scope of this work.

In this study, we have shown that ultralow-pinning Pt/CoFeB/MgO multilayer stacks exhibit several distinct morphological phases whose stability is dictated by temperature

[2] Such phase transformation can generally be attributed to the class of continuous transformations with the local magnetization being a nonconserved order parameter [32]

[3] A theoretical upper bound for $\Delta T^{\max}_{\text{Joule}}$ is $\sim 100\ K$, which can be estimated from a tabulated thermal capacity, and known mass of Pt layers after considering that a single 1.0 V 5 ns pulse is transmitted through our 50 Ω multilayer wires and assuming that all the Joule heating reaches Pt layers.

and applied field. Transitions between phases can be triggered by transient heating due to current-pulse injection which, in combination with the applied field amplitude, allow us to select desired phases and create magnetic skyrmions on demand. As opposed to skyrmion generation enabled by defects [16, 24, 25], these intrinsic phase transitions may be more desirable in practice, as defect centers can act as pinning sites that subsequently impede motion of skyrmions in devices. We demonstrate that in this material, an entire array of skyrmions can be generated reliably with just a single few-nanosecond-long pulse. Finally, we establish multiple ways to obtain the zero-field skyrmions that can be readily manipulated by current. Our findings provide new fundamental insights and reveal new mechanisms for the creation of skyrmions and their deterministic motion, which are essential ingredients for future spintronic applications.

METHODS

Experimental methods

Multilayer films of $[\text{Pt}(2.7\text{ nm})/\text{CoFeB}(0.86\text{ nm})/\text{MgO}(1.5\text{ nm})]_{\times 15}$ with Pt(2.7 nm) capping layer were grown on SiN membranes with an underlayer of Ta(3.6 nm)/Pt(1.0 nm) (required for better adhesion) using Magnetron Sputter deposition with Ar pressure of 3.0 mTorr and background pressure of 0.5 μTorr. The dead layer thickness of the magnetic material $t_{\text{dead layer}} \approx 0.09$ nm, was found by comparing the saturation magnetization in grown multilayer films with different thicknesses of CoFeB (so the actual magnetic thickness of CoFeB is 0.77 nm). The 2 μm$\times$5μm wires have been patterned using electron beam lithography and lift-off procedure. The measured resistance of the wires is $\sim 50\ \Omega$ at room temperature. Magnetic film parameters were measured by using a vibrating sample magnetometer (VSM) on continuous films, resulting in $M_s = 1.12 \times 10^6\,\text{A/m}$, $K_{\text{eff}} = 1.9 \times 10^5\,\text{J/m}^3$ ($K_u = 9.78 \times 10^5\,\text{J/m}^3$), DMI $= 1.15 \times 10^{-3}\,\text{J/m}^2$ (assuming $A = 1.0 \times 10^{-11}\,\text{J/m}$). The DMI constant has been extracted by comparing the multidomain states in grown films with micromagnetic simulations and verified by the exact multilayer multidomain theory [36].

The imaging of wires was carried out using scanning transmission X-ray microscopy (STXM) at the MAXYMUS beamline at the BESSY II synchrotron in Berlin, Germany and STXM microscopy at the PolLux (X07DA) [37] beamline at the Swiss Light Source in

Villigen, Switzerland.

Simulation methods

Micromagnetic simulations were employed using Mumax3 [38] and MicroMagnum [4] (for Supplemetary section) micromagnetic software. The simulation parameters were obtained from the experimentally measured magnetic parameters by following the effective medium approach [4, 36, 39], in which the magnetic parameters of multilayers are effectively scaled. Single layer grid of 2598×3000 with the cell size of 3 nm $\times$ 3 nm $\times$ 75.4 nm and periodic boundary conditions (PBC) were applied. A slight deviation from a square simulation size was required to fit a trigonal skyrmion lattice to PBC conditions. Note that even though we simulated an infinite-like system, our results are general and can be applied for micron-wide wires as well. As we find from micromagnetic simulations, finite size effects, such as the repulsion of magnetic textures from the wire edges, represent a second order effect that keeps our energetics arguments valid (finite size effects, however, can contribute to the orientation of stripe alignment, see Supplement for details). Stripes (skyrmion lattice) states have been obtained by using a relaxation procedure on the simulation samples with different densities of domains (skyrmions). After comparing the energies, the minimum energy state was found. The labyrinth states were initialized by relaxing the sample with random initial magnetization. For plotting the magnetization distribution in Fig. 4a-c, Muview2 [5] 3D visualization software was used.

ACKNOWLEDGEMENTS

This work was supported by the U.S. Department of Energy (DOE), Office of Science, Basic Energy Sciences (BES) under Award #DE-SC0012371. M.K. and the group at Mainz acknowledge support by the DFG (in particular SFB TRR173 Spin+X), the Graduate School of Excellence Materials Science in Mainz (MAINZ, GSC 266), the EU (MultiRev (ERC-2014-PoC 665672), WALL (FP7-PEOPLE-2013-ITN 608031)), SpinNet, a topical network project of the German Academic Exchange Service (DAAD), and the Research Center of Innovative and Emerging Materials at Johannes Gutenberg University (CINEMA). K.L.

[4] micromagnum.informatik.uni-hamburg.de

[5] grahamrow.github.io/Muview2/

gratefully acknowledges financial support by the Graduate School of Excellence Materials Science in Mainz (MAINZ). K.L. and N.K. gratefully acknowledge financial support of the German Academic Scholarship Foundation. F.B. acknowledges financial support by the German Research Foundation through grant no. BU 3297/1-1. The PolLux endstation was financed by the German Minister für Bildung und Forschung (BMBF) through contracts 05KS4WE1/6 and 05KS7WE1. M.-Y.I. acknowledges support by the DGIST R&D program of the Ministry of Science, ICT and future Planning (17-BT-02).

AUTHOR CONTRIBUTIONS

I.L. and G.S.D.B. conceived the project. M.K. and G.S.D.B. supervised the project. I.L. and K.L. fabricated samples and derived the introduced concepts of the phase transition mechanisms. I.L. performed sample characterization. K.L., D.H., and J.Z. performed sample heating measurements. I.L., K.L., P.B., N.K., and M.W. conducted STXM experiments at the MAXYMUS beamline at the BESSY II synchrotron in Berlin. I.L., K.L., P.B., D.H., S.F., and J.R. performed X-ray imaging experiments using STXM microscopy at the PolLux (X07DA) beamline at the Swiss Light Source in Villigen, Switzerland. I.L., K.L., F.B., L.C., M.M., and M.-Y.I. performed X-ray imaging experiments using Magnetic Transmission X-ray Microscopy (MTXM) at the Advanced Light Source in Berkeley, California. I.L. and K.L. performed and analysed the micromagnetic simulations and wrote the Supplementary Information. I.L. drafted the manuscript. All authors discussed the results, the implications, and the figures and commented on the manuscript.

[1] Jeong, T. & Pickett, W. E. Implications of the B20 crystal structure for the magnetoelectronic structure of MnSi. *Physical Review B - Condensed Matter and Materials Physics* **70** (2004).

[2] Mühlbauer, S. *et al.* Skyrmion Lattice in a Chiral Magnet. *Science* **323**, 915–920 (2009).

[3] Yu, X. Z. *et al.* Real-space observation of a two-dimensional skyrmion crystal. *Nature* **465**, 901–904 (2010).

[4] Woo, S. *et al.* Observation of room-temperature magnetic skyrmions and their current-driven dynamics in ultrathin metallic ferromagnets. *Nature Materials* **15**, 501–506 (2016).

[5] Moreau-Luchaire, C. *et al.* Additive interfacial chiral interaction in multilayers for stabilization of small individual skyrmions at room temperature. *Nature Nanotechnology* **11**, 731 (2016).

[6] Boulle, O. *et al.* Room-temperature chiral magnetic skyrmions in ultrathin magnetic nanostructures. *Nature Nanotechnology* **11**, 449–454 (2016).

[7] Romming, N., Kubetzka, A., Hanneken, C., Von Bergmann, K. & Wiesendanger, R. Field-dependent size and shape of single magnetic skyrmions. *Physical Review Letters* **114**, 177203 (2015).

[8] Jiang, W. *et al.* Direct observation of the skyrmion Hall effect. *Nature Physics* **13**, 162–169 (2016).

[9] Litzius, K. *et al.* Skyrmion hall effect revealed by direct time-resolved x-ray microscopy. *Nature Physics* **13**, 170–175 (2016).

[10] Zhang, X., Ezawa, M. & Zhou, Y. Magnetic skyrmion logic gates: conversion, duplication and merging of skyrmions. *Scientific Reports* **5**, 9400 (2015).

[11] Fert, A., Cros, V. & Sampaio, J. Skyrmions on the track. *Nature Nanotechnology* **8**, 152–156 (2013).

[12] Dzyaloshinsky, I. A thermodynamic theory of "weak" ferromagnetism of antiferromagnetics. *Journal of Physics and Chemistry of Solids* **4**, 241–255 (1958).

[13] Moriya, T. Anisotropic superexchange interaction and weak ferromagnetism. *Physical Review* **120**, 91–98 (1960).

[14] Tomasello, R. *et al.* A strategy for the design of skyrmion racetrack memories. *Scientific reports* **4**, 6784 (2014).

[15] Legrand, W. *et al.* Room-temperature current-induced generation and motion of sub-100 nm skyrmions. *Nano Letters* **17**, 2703–2712 (2017).

[16] Büttner, F. *et al.* Field-free deterministic ultra fast creation of skyrmions by spin orbit torques. *arXiv* 1705.01927 (2017).

[17] Romming, N. *et al.* Writing and deleting single magnetic skyrmions. *Science* **341**, 636–639 (2013).

[18] Sampaio, J., Cros, V., Rohart, S., Thiaville, A. & Fert, A. Nucleation, stability and current-induced motion of isolated magnetic skyrmions in nanostructures. *Nature nanotechnology* **8**, 839–844 (2013).

[19] Cape, J. A. & Lehman, G. W. Magnetic domain structures in thin uniaxial plates with perpendicular easy axis. *Journal of Applied Physics* **42**, 5732–5756 (1971).

[20] Muratov, C. B. Theory of domain patterns in systems with long-range interactions of Coulomb type. *Physical Review E - Statistical, Nonlinear, and Soft Matter Physics* **66**, 066108 (2002).

[21] Jiang, W. *et al.* Blowing magnetic skyrmion bubbles. *Science* **349**, 283–286 (2015).

[22] Heinonen, O., Jiang, W., Somaily, H., Te Velthuis, S. G. E. & Hoffmann, A. Generation of magnetic skyrmion bubbles by inhomogeneous spin Hall currents. *Physical Review B - Condensed Matter and Materials Physics* **93** (2016).

[23] Müller, J. & Rosch, A. Capturing of a magnetic skyrmion with a hole. *Physical Review B - Condensed Matter and Materials Physics* **91** (2015).

[24] Sitte, M. *et al.* Current-driven periodic domain wall creation in ferromagnetic nanowires. *Physical Review B* **94** (2016).

[25] Everschor-Sitte, K., Sitte, M., Valet, T., Sinova, J. & Abanov, A. Skyrmion production on demand by homogeneous DC currents. *arXiv* 1610.08313 (2016).

[26] Woo, S. *et al.* Spin-orbit torque-driven skyrmion dynamics revealed by time-resolved X-ray microscopy. *Nature Communications* **8**, 15573 (2017).

[27] Emori, S., Bauer, U., Ahn, S.-M., Martinez, E. & Beach, G. S. D. Current-driven dynamics of chiral ferromagnetic domain walls. *Nature Materials* **12**, 611–616 (2013).

[28] Sinova, J., Valenzuela, S. O., Wunderlich, J., Back, C. H. & Jungwirth, T. Spin Hall effects. *Reviews of Modern Physics* **87**, 1213–1260 (2015).

[29] Rohart, S. & Thiaville, A. Skyrmion confinement in ultrathin film nanostructures in the presence of Dzyaloshinskii-Moriya interaction. *Physical Review B - Condensed Matter and Materials Physics* **88** (2013).

[30] Seul, M. & Andelman, D. Domain shapes and patterns: the phenomenology of modulated phases. *Science* **267**, 476–483 (1995).

[31] Montoya, S. A. *et al.* Tailoring magnetic energies to form dipole skyrmions and skyrmion lattices. *Physical Review B* **95**, 024415 (2017).

[32] Balluffi, R. W., Allen, S. M. & Carter, W. C. *Kinetics of Materials* (2005).

[33] Zavadskii, E. A. & Zablotskii, V. A. Phase Transition in Magnetic Bubble Lattices. *Physica Status Solidi (a)* **112**, 145–153 (1989).

[34] Seul, M. & Wolfe, R. Evolution of disorder in magnetic stripe domains. I. Transverse instabilities and disclination unbinding in lamellar patterns. *Physical Review A* **46**, 7519–7533 (1992).

[35] Garel, T. & Doniach, S. Phase transitions with spontaneous modulation-the dipolar Ising ferromagnet. *Physical Review B* **26**, 325–329 (1982).

[36] Lemesh, I., Büttner, F. & Beach, G. S. D. Accurate model of the stripe domain phase of perpendicularly magnetized multilayers. *Physical Review B* **95**, 174423 (2017).

[37] Raabe, J. *et al.* PolLux: A new facility for soft x-ray spectromicroscopy at the swiss light source. *Review of Scientific Instruments* **79** (2008).

[38] Vansteenkiste, A. *et al.* The design and verification of MuMax3. *AIP Advances* **4**, 107133 (2014).

[39] Suna, A. Perpendicular magnetic ground state of a multilayer film. *Journal of Applied Physics* **59**, 313–316 (1986).